Arctic Sea Level Variations in Nares Strait 2003-12

Andreas Münchow *

University of Delaware, Newark, Delaware

Co-Author(s)

ABSTRACT

[Jan.-2, 2015]

1. Introduction

The southward flow of fresh and icy waters from the Arctic to the North-Atlantic Ocean has saved many sailor's lives after their ships were crushed and wrecked by mobile ice in Nares Strait to the west of northern Greenland (Dick 2001). Those who escaped did so by surviving on large and thick ice floes that advected along the eastern coasts of Canada from Ellesmere Island at 81N latitude to Labrador near 53N latitude (Hendrik 1878). More controlled ocean experiments were conducted by the US Coast Guard at the height of the Cold War when Thule Air Force Base and Early Warning radar sites were established to detect and intercept missiles and aircraft (). First publications on the oceanography of Nares Strait described the movement of Ward Hunt ice island from northern Ellesmere Island to Labrador (Nutt 1966), the movement of ice with airborne radar observations (Dunbar 1973), and the movement of ocean waters with month-long moored sensors (Sadler 1976). Motivated by these sketchy observations LeBlond (1980) applied geostrophic constraints to diagnose surface currents in the Canadian Arctic Archipelago and Nares Strait as a baroclinic circulation with flows in opposite directions on opposing sides of channels and straits.

Remote sensing studies such as Steffen (1985) and later Vincent et al. (2008) focused on the so-called North Water (NOW) polynya at the southern entrance to Nares Strait. In most years the southward advection of Arctic sea ice comes to a complete stop for several months in winter when the ice forms a stable arching mass that is attached solidly to the coasts of both the Greenland and Ellesmere Island (Kwok 2005; Dumont et al. 2009). Ice motion vectors for the area are presented by Wilson et al. (2001) that suggest southward advection away from the ice arch driven by winds and ocean currents. Melling et al. (2001) report moored ocean current observations from 1997 to 1998 for the NOW polynya area that suggest a southward flow along Ellesmere Island and a northward flow along Greenland, but gaps in time and space prevented firm conclusions. Large spatial and temporal ocean variability resulted in large uncertainties of estimated statistical and dynamical properties.

Nevertheless, all studies reveal a generally southward flux of ice and water that was first quantified at interannual time scales by Münchow and Melling (2008) and Rabe et al. (2012) from a large moored array deployed in Nares Strait from 2003 through 2006. They found mean volume and freshwater flux during that period of 0.72 ± 0.11 Sv (10^6 m^3/s) and 28 ± 3 mSv from records of ocean current (Münchow and Melling 2008), temperature, salinity, and pressure (Rabe et al. 2012). Along with synoptic ship-based surveys of velocity and density fields (**?**) these authors find dynamical balances that appear geostrophic in the across-channel and pressure-gradient driven in the along-channel direction. More specifically, the along-channel difference of observed bottom pressure fluctuations was highly coherent with observed volume flux fluctuations from 2003 to 2006. We here will expound this initial result by presenting and analyzing bottom pressure and temperature records for the entire 2003 to 2012 period as we successfully recovered an active sensor in August of 2012 with a complete 9-year data record.

2. Study Area, Data, and Methods

In 2003 we deployed five pressure recorders in shallow bays of Nares Strait, a generally ice-covered 30-50 km wide and 500 km long strait that connects the Arctic Ocean in the north to Baffin Bay in the south to the west of Greenland. Two pressure recorders were recovered in 2006 at the southern end of the strait, at Foulke Fjord, Greenland (78.30N, 72.57W) and at Alexandra Fjord, Canada (78.91N, 75.80W), two were lost, and the last was recovered in 2012 at Discovery Harbor, Canada (81.71N, 64.80W) after recovery attempts in 2005, 2006, 2007, and 2009 all failed to retrieve the instrument.

We mounted instruments to a stainless-steel stake that divers drove into the consolidated sediment several feet beneath the seabed. The stake supported the full weight of the instrument package, thereby minimizing subsidence caused by insufficient bearing strength of the surface sediments and by wave scouring (Münchow and Chant 2000).

All recorders contained Digiquartz pressure sensors (Paroscientific Inc.) that resolve signals better than 0.1 mb or about 1 mm of sea level. We recorded 30 one second samples every three hours with the least significant bit representing 0.76 mbar. The largest error results from quantization and is about 0.22 mbar estimated by using a procedure outlined by Bendat and Piersol (1986) on page 340. This value is close the white spectral noise floor that we find from a 9-year record near 0.32 mbar corresponding to 10^{-3} cm^2 cpd^{-1}. This white sensor noise is distinct and separate from red noise, to be discussed later, of the environment where our instruments are deployed.

Subsequent deployments at Alexandra Fjord used the more common method of attaching the pressure sensor to an anchor placed at the surface of the bottom. New firmware decreased the digital quantization error by more than an order of magnitude and the largest error source now are small anchor shifts as the instrument settles into the sediment or is moved by deep ice keeps reaching the bottom. We identified several distinct anchor shifts of 0.2 to 0.8 db due to dragging of the sensor package by ice. We removed these offsets by manual adjustments.

The 2003-12 Discovery Harbor record contained intermittent gaps after 2008 which we filled using a linear transfer function H(f) derived from the 2003-06 common record of Alexandra Fjord (AF) and Discovery Harbor (DH), .e.g.,

$$Y_{DH}(f) = H(f) \times X_{AF}(f) \tag{1}$$

where X_{AF} and Y_{DH} are Fourier transforms of bottom pressure and f is a frequency. Assuming stationarity, we apply the 2003-06 transfer function to 2008-12 observations from Alexandra Fjord to estimate $Y_{DH}(f)$ which is then transformed back into the time domain to fill missing values.

We also use sea-level data from a tide gauge operated by the Canadian Hydrographic Service at Alert, Canada just west of the northern end of the Nares Strait (82.49N, 62.32W). These data are corrected for the inverted barometer effect (Neumann and Pierson 1966) using sea-level pressure data.

Data from these four stations provide first estimates of along- and across-channel pressure and pressure differences from tidal to interannual time scales in the area shown in Figure-1 that we discuss next.

3. Tides

Tidal oscillations constitute the main source of variability in Nares Strait (Münchow and Melling 2008). Our long record

4. Pressure Gradients

5. Discussion and Conclusions

It should be noted, however, that the buoyant waters often reside on shelves and slopes, hence across-shelf exchange and mixing processes must export such waters from shallow to deep water to reduce vertical stratification in regions of deep convection such as takes place over the deep basins of the Greenland and Labrador Seas. The buoyant along-shore flows often follow sloping topographies and are approximately in baroclinic geostrophic balance. Nevertheless, it is unclear what drives these flow.

Frictional surface stresses imposed by the winds are active year-round in Fram Strait where the ice is mobile, but they are less important in Nares Strait that is covered by land-fast ice for most of the year. The role of barotropic along-shore pressure gradients is less clear as they are often unpractical to measure along indented complex coastlines in remote regions. Nevertheless, such pressure gradients play an often dominant role in coastal areas near sloping topographies as has been demonstrated by **?** and **?**Chapman1992) for the continental shelf and slope areas off the US West Coast and East Coasts, respectively.

A linear regression of sea level with time gives -0.15 ± 0.85 mm per year which is indistinguishable from zero. The uncertainty is a 95 % confidence limit using a 10-day decorrelation time scale to estimate degrees of freedom. A similar regression of bottom temperature gives $+0.53 \pm 0.32$ mK. The significant warming trend is exceedingly small, about 0.1 K in 200 years that for practical purposes is zero.

Acknowledgments.

The National Science Foundation supported the initial fieldwork with Grant 0230236 (AM and HM) while the analyses were supported by 1022843 (AM). The Canadian Department of Fisheries and Oceans and University of Delaware supported this study with salaries, institutional, and logistical infrastructure.

APPENDIX

Something

REFERENCES

Bendat, J. and A. Piersol, 1986: *Random data: analysis and measurement procedures*. 2d ed., John Wiley & Sons, New York, NY, 566 pp.

Dick, L., 2001: *Muskox Land, Ellesmere Island in the age of contact*. University of Calgary Press, Calgary, Alberta, 615 pp.

Dumont, D., Y. Gratton, and T. E. Arbetter, 2009: Modeling the dynamics of the North Water polynya ice bridge. *J. Phys. Oceanogr.*, **39 (6)**, 1448–1461.

Dunbar, M., 1973: Ice regime and ice transport in Nares Strait. *Arctic*, **26 (4)**, 282–291.

Hendrik, H., 1878: *Memoirs of Hans Hendrik, the Arctic traveler, serving under Kane, Hall, and Nares 1853-1876*. Truebener and Co., London.

Kwok, R., 2005: Variability of Nares Strait ice flux. *Geophys. Res. Let.*, **32 (24)**, L24 502, doi:10.1029/2005GL024768.

LeBlond, P. H., 1980: On the surface circulation in some channels of the Canadian Arctic Archipelago. *Arctic*, **33 (1)**, 189–197.

Melling, H., Y. Gratton, and G. Ingram, 2001: Ocean circulation within the North Water polynya of Baffin Bay. *Atmos.-Oceans*, **39 (3)**, 301–325.

Münchow, A. and R. J. Chant, 2000: Kinematics of inner shelf motions during the summer stratified season off New Jersey. *J. Phys. Oceanogr.*, **30 (2)**, 247–268.

Münchow, A., K. Falkner, and H. Melling, 2007: Spatial continuity of measured seawater and tracer fluxes through Nares Strait, a dynamically wide channel bordering the Canadian Archipelago. *J. Mar. Res.*, **65 (6)**, 759–788.

Münchow, A., R. W. Garvine, and T. F. Pfeiffer, 1992: Subtidal currents from a shipboard acoustic doppler current profiler in tidally dominated waters. *Cont. Shelf Res.*, **12 (4)**, 499–515.

Münchow, A. and H. Melling, 2008: Ocean current observations from Nares Strait to the west of Greenland: Interannual to tidal variability and forcing. *J. Mar. Res.*, **66 (6)**, 801–833.

Neumann, G. and W. J. Pierson, 1966: *Principles of Physical Oceanography*. Prentice-Hall Inc., 545pp pp.

Nutt, D. C., 1966: Drift of ice island WH-5. *Arctic*, **19 (3)**, 244–262.

Padman, L. and S. Erofeeva, 2004: A barotropic inverse tidal model for the Arctic Ocean. *Geophys. Res. Let.*, **31 (2)**, L02 303, doi:10.1029/2003GL019003.

Rabe, B., H. Johnson, A. Münchow, and H. Melling, 2012: Geostrophic currents and freshwater fluxes through Nares Strait to the west of northern Greenland. *J. Mar. Res.*, **70**, 603–640.

Sadler, H., 1976: Water, heat, and salt transport through Nares Strait, Ellesmere Island. *J. Fish. Res. Board Can.*, **33**, 2286–2295.

Steffen, K., 1985: Warm water cells in the NORTH WATER, northern BAFFIN-BAY during winter. *J. Geophys. Res.*, **90 (NC5)**, 9129–9136, doi:10.1029/JC090iC05p09129.

Vincent, R. F., R. F. Marsden, P. J. Minnett, K. A. M. Creber, and J. R. Buckley, 2008: Arctic waters and marginal ice zones: A composite Arctic sea surface temperature algorithm using satellite thermal data. *Journal of Geophysical Research-oceans*, **113 (C4)**, C04 021.

Wilson, K., D. Barber, and D. King, 2001: Validation and production of RADARSAT-1 derived ice-motion maps in the North Water (NOW) polynya, january-december 1998. *Atmosphere-Ocean*, **39 (3)**, 257–278.

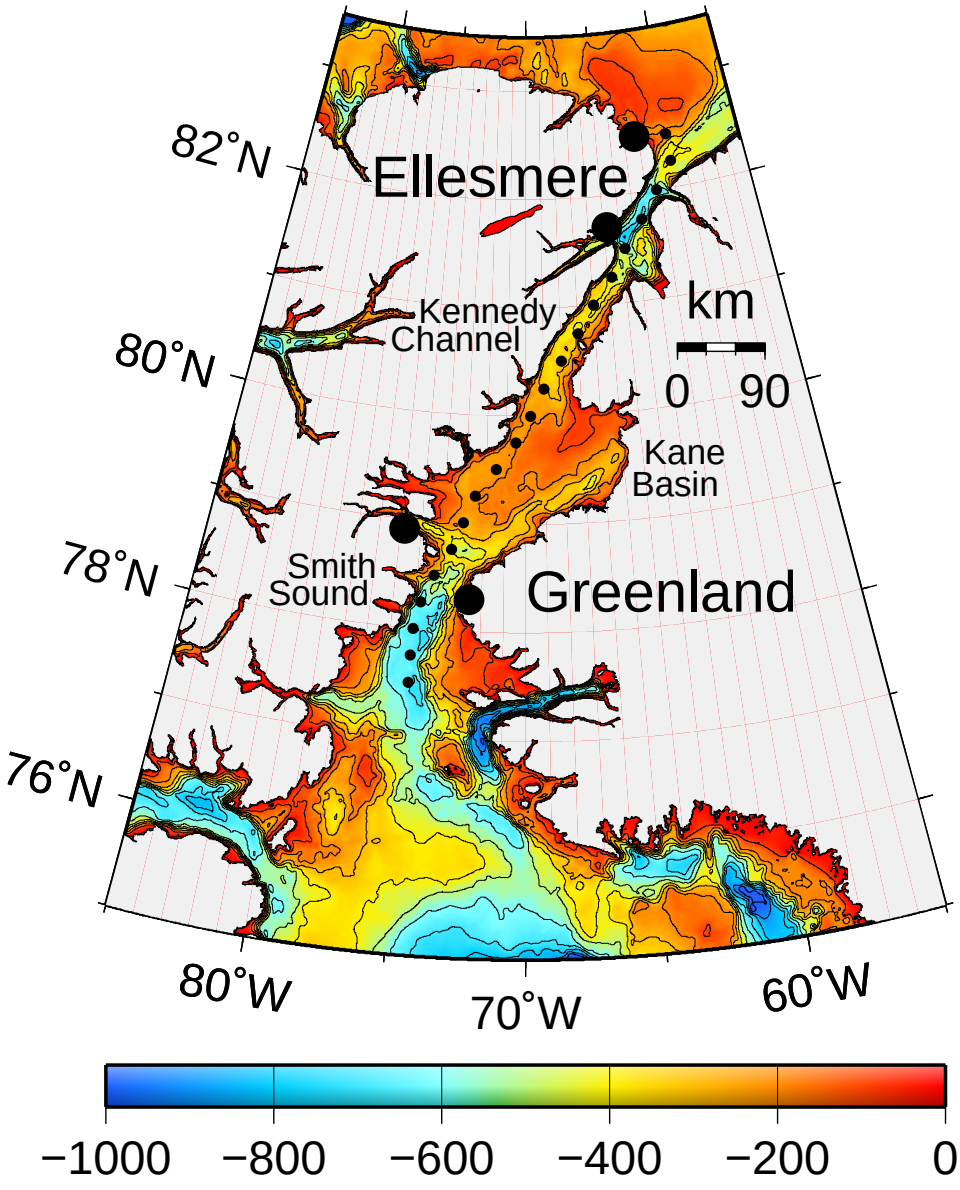

FIG. 1. Map of the Study area. Colors represent bottom depths in meters, large dots locate time series of sea level and bottom pressure observations, while small dots indicate locations of tidal properties taken from Padman and Erofeeva (2004) for comparison.

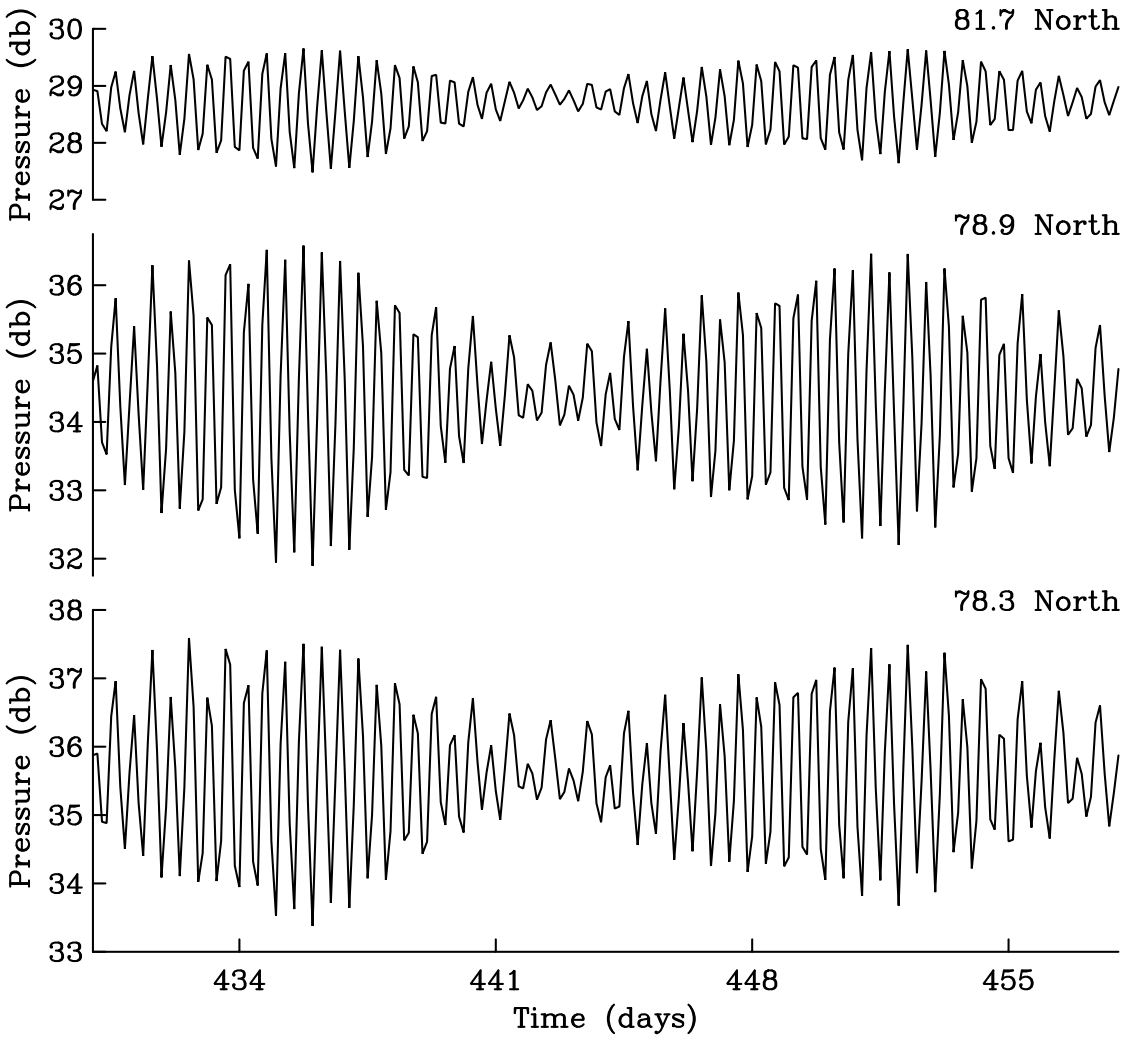

FIG. 2. A 28-day segment of raw bottom pressure data at Discovery Harbor (top), Alexandra Fjord (middle), and Folke Fjord (bottom) in March of 2004.

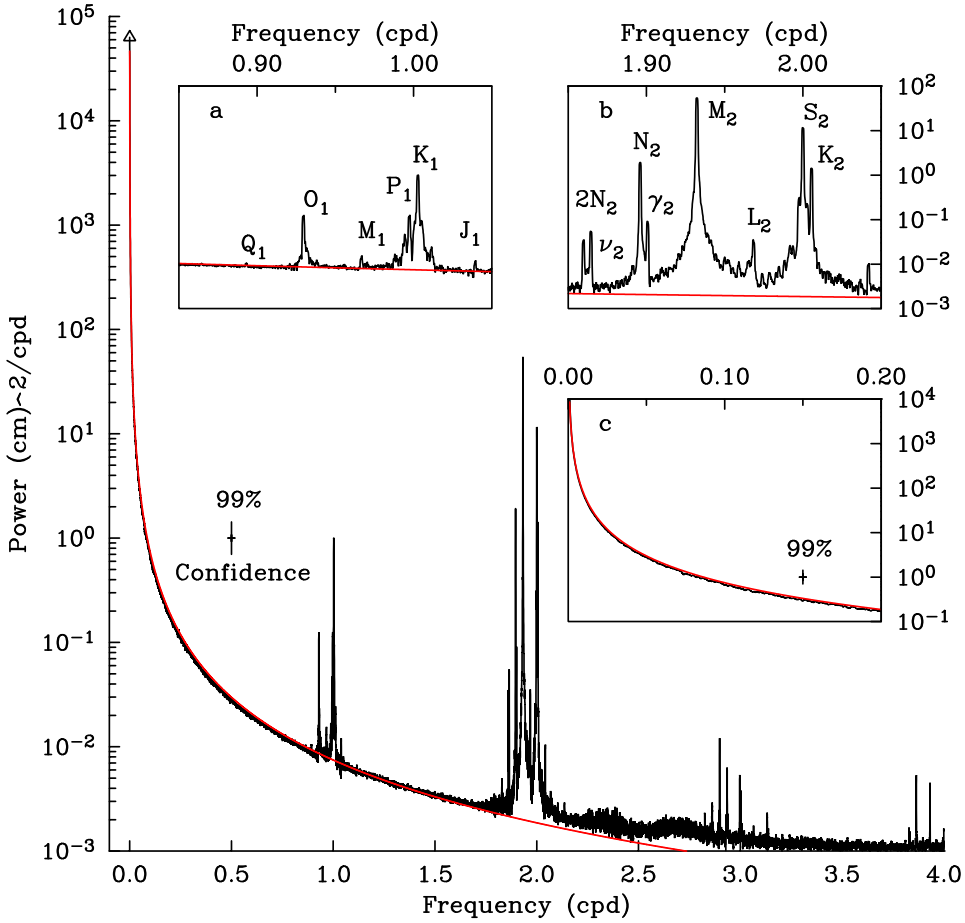

FIG. 3. Spectra of bottom pressure at Discovery Harbor for a record from 2003 to 2012. Inserts expand (a) diurnal, (b) semi-diurnal, and (c) subtidal frequency bands. Red line indicates modeled red power spectra.

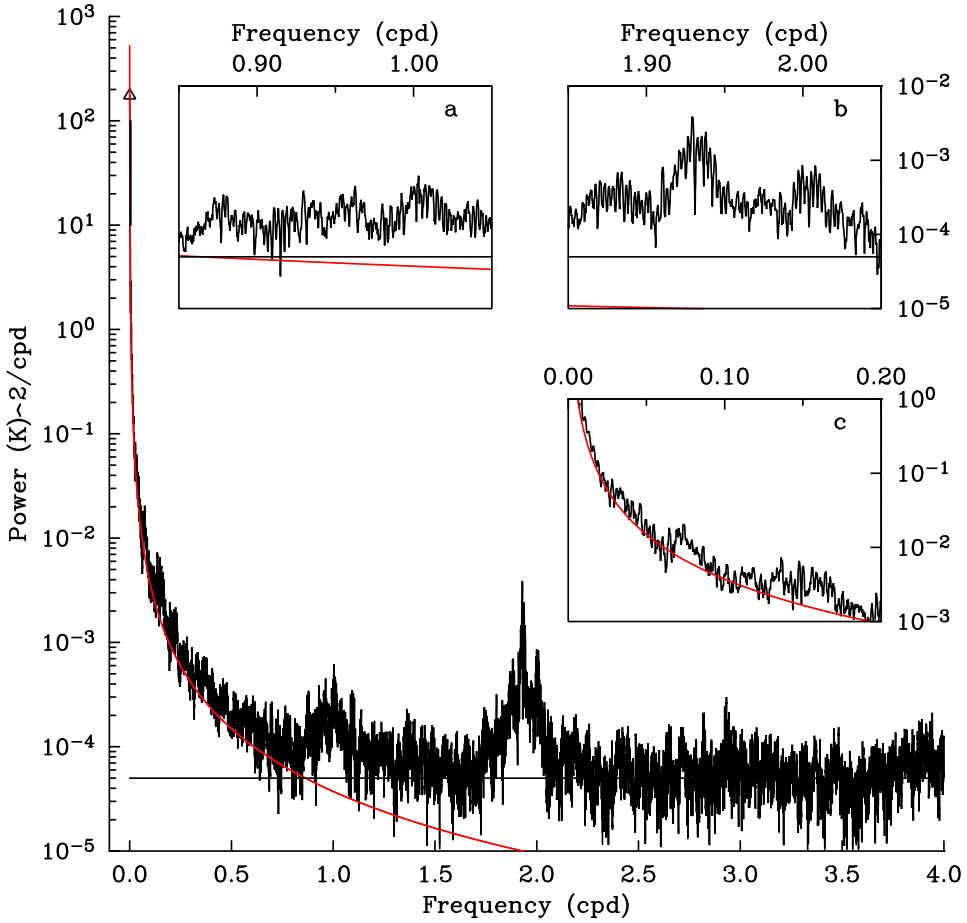

FIG. 4. Spectra of bottom temperature at Discovery Harbor for a record from 2003 to 2012. Inserts expand (a) diurnal, (b) semi-diurnal, and (c) subtidal frequency bands. Red line indicates modeled red power spectra.

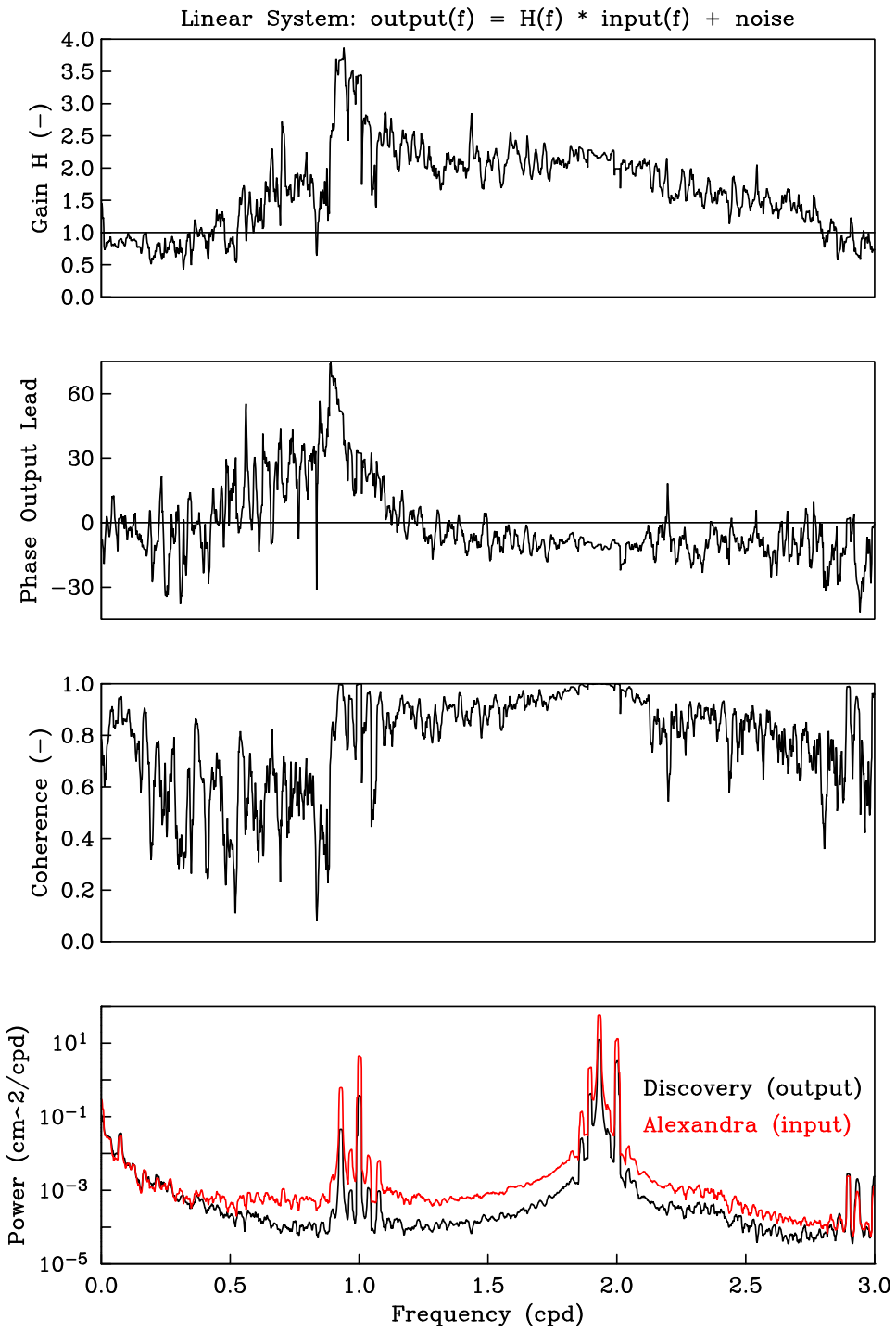

FIG. 5. Power spectra of bottom pressure at Discovery Harbor and Alexandra Fjord for a record from 2003 to 2012 along with coherence and transfer function (phase and gain) between these two time series in the frequency domain.

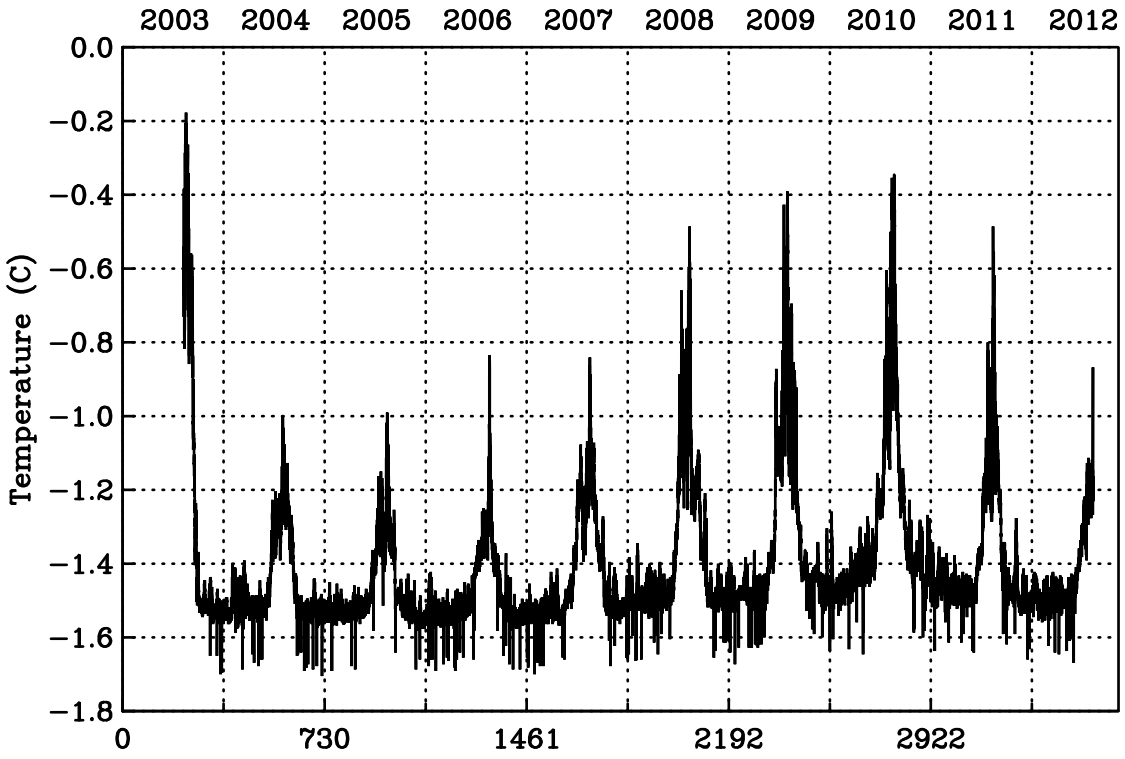

FIG. 6. Time series of ocean temperature at 30-m depth in Discovery Harbor.

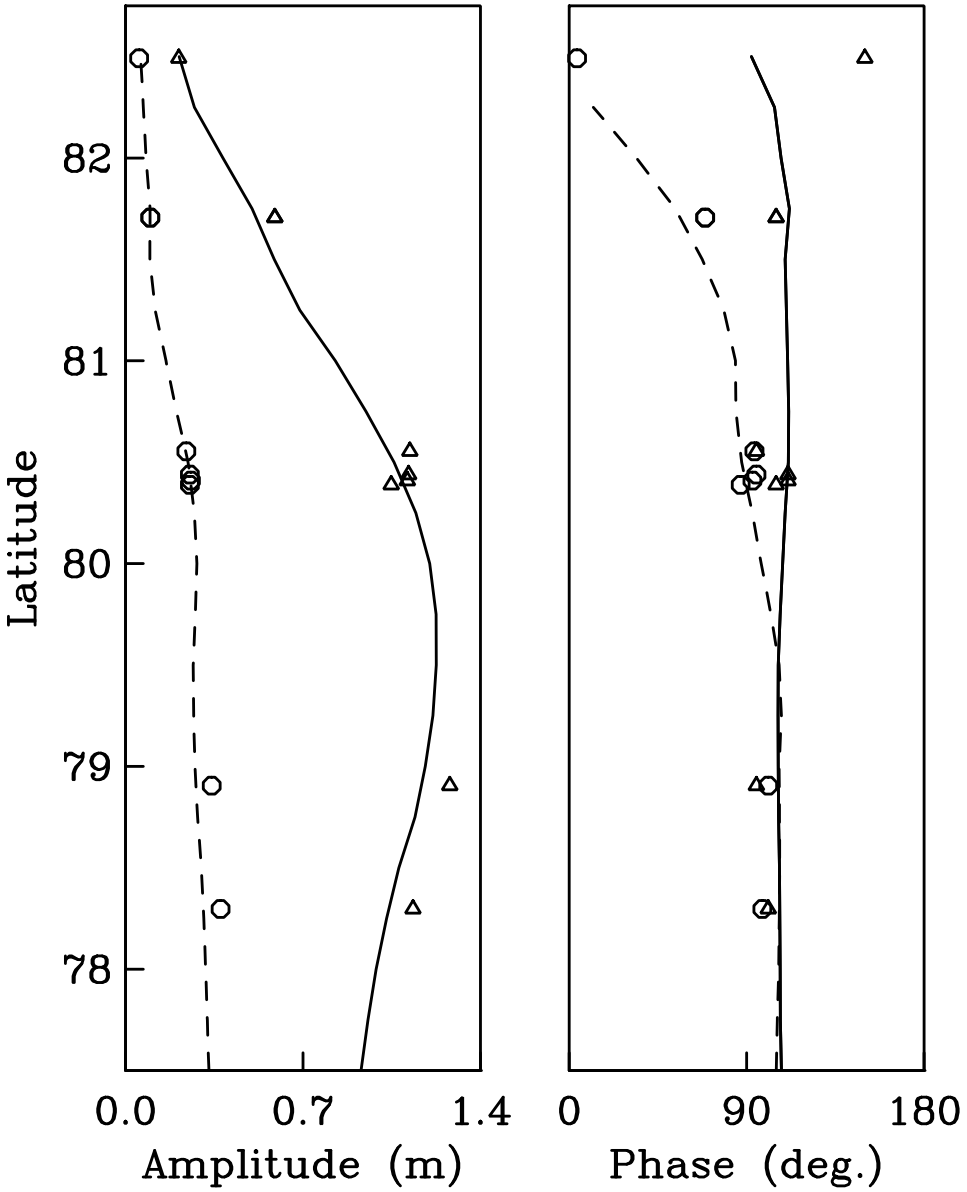

FIG. 7. Comparison of M_2 (solid, triangles) and K_1 (dashed, circles) amplitude (left panel) and phase (right panel) from observations (symbols) and model (line) predictions of Padman and Erofeeva (2004).

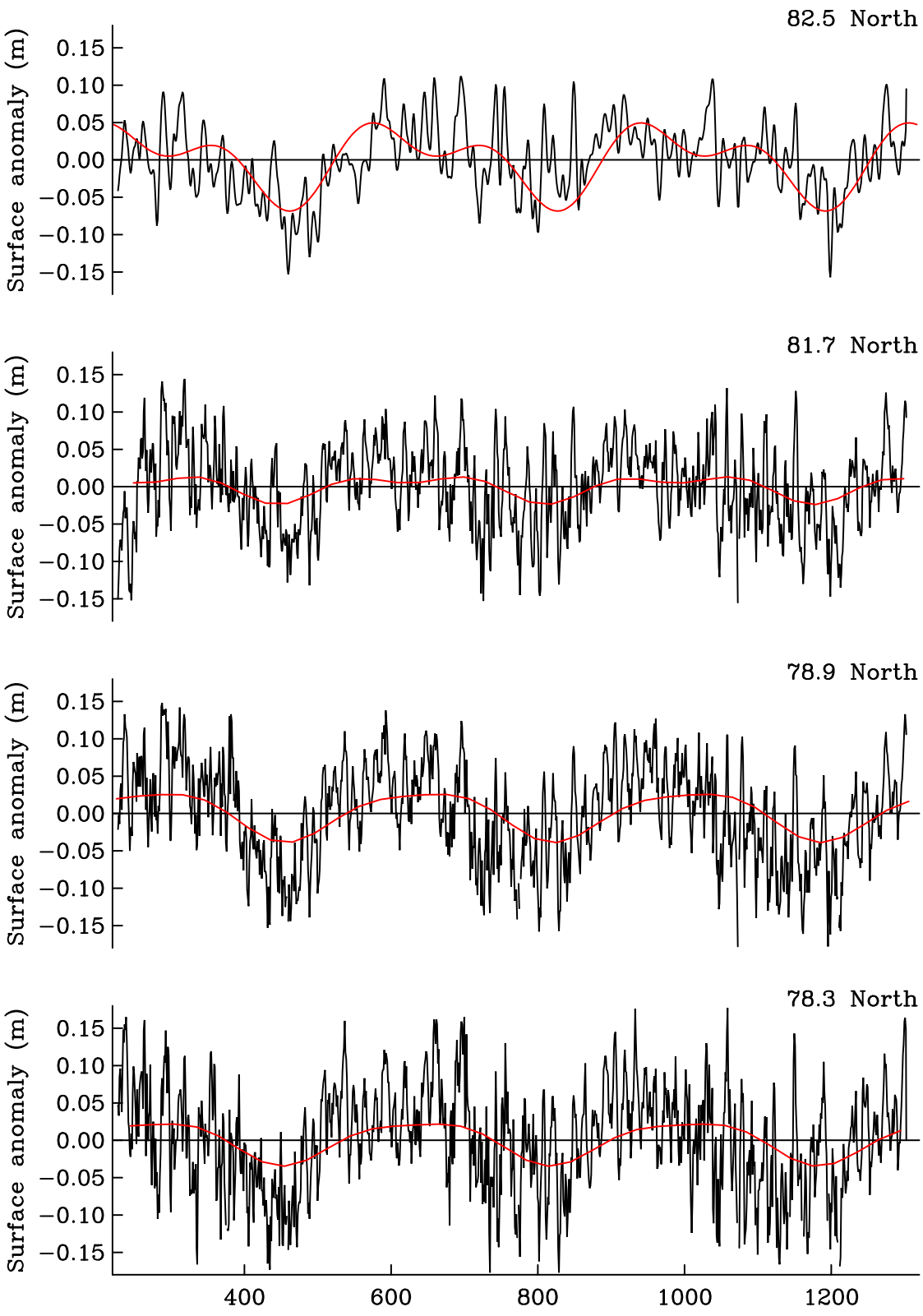

FIG. 8. Low-pass filtered (non-tidal) bottom pressure fluctuations along Nares Strait from north (top) to south (bottom) for the common 2003-06 period.

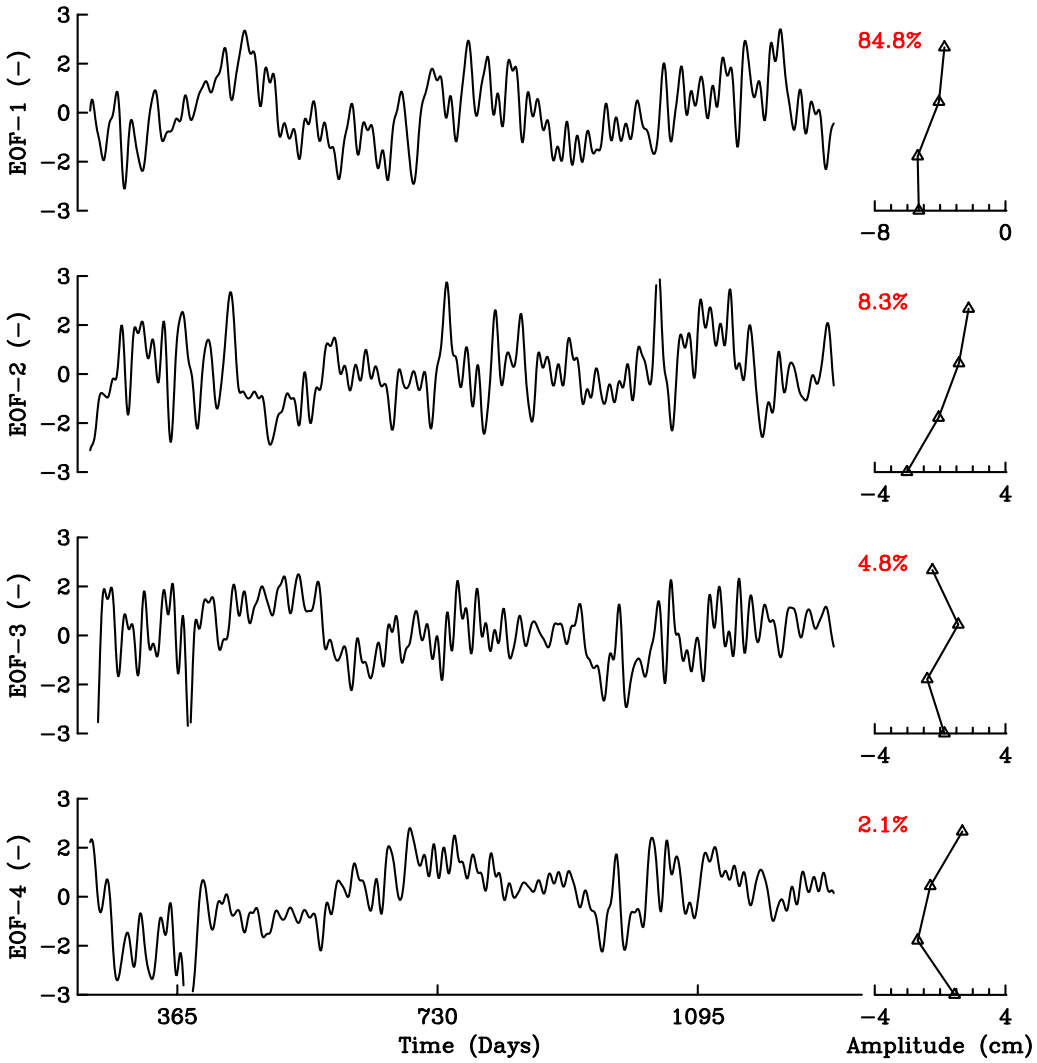

FIG. 9. Empirical orthogonal functions of low-pass filtered (non-tidal) bottom pressure fluctuations. Temporal fluctuations (left panel) are scaled to have unit standard deviations while spatial fluctuations (right panel) along Nares Strait are amplitudes for each of 4 stations from Alert in the north (top) to Foulke Fjord in the south (bottom) that modulate the temporal fluctuations.

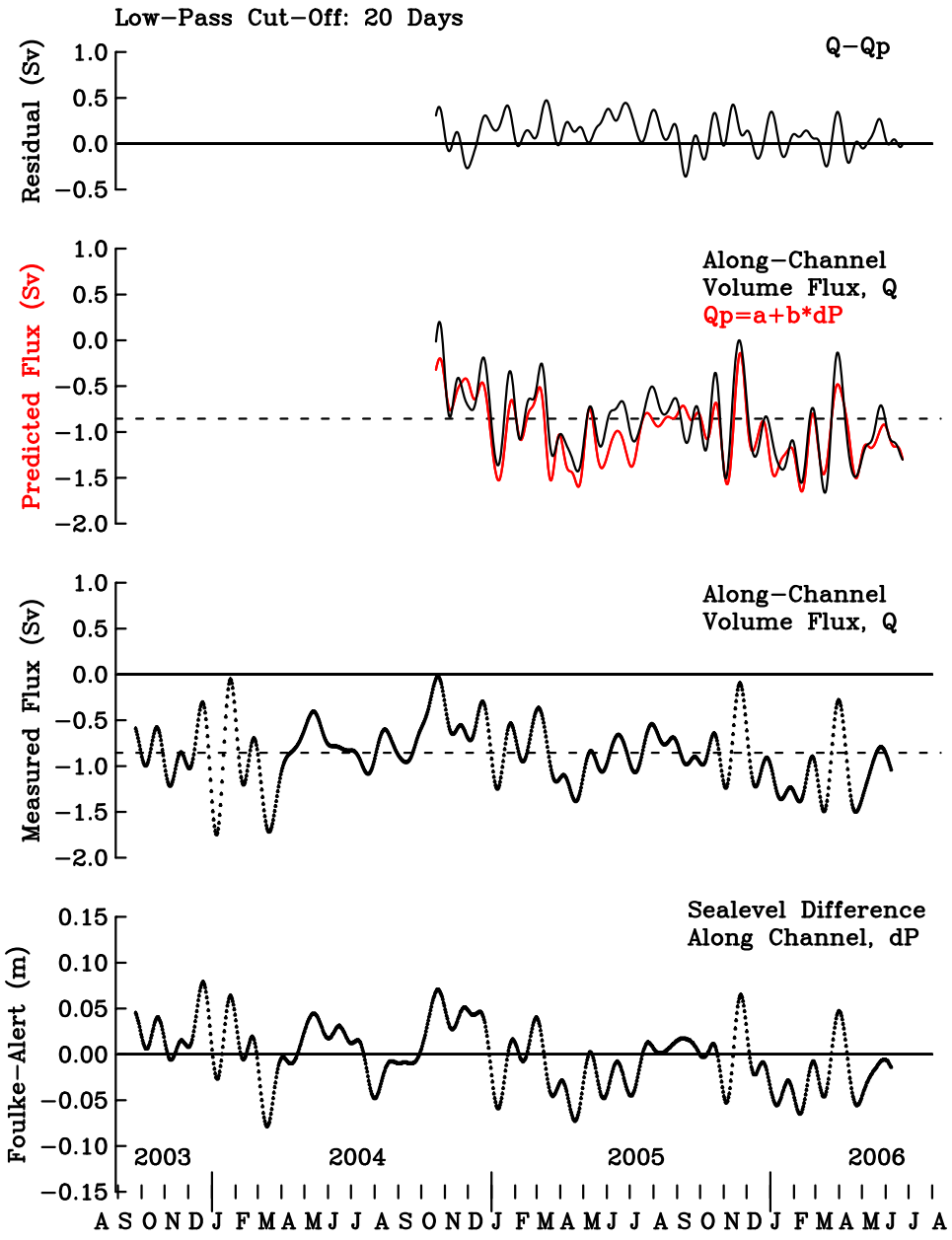

FIG. 10. Regression of along-channel pressure difference with volume flux. The regression is erived for the 2003/04 data and applied to the 2005/06 data.

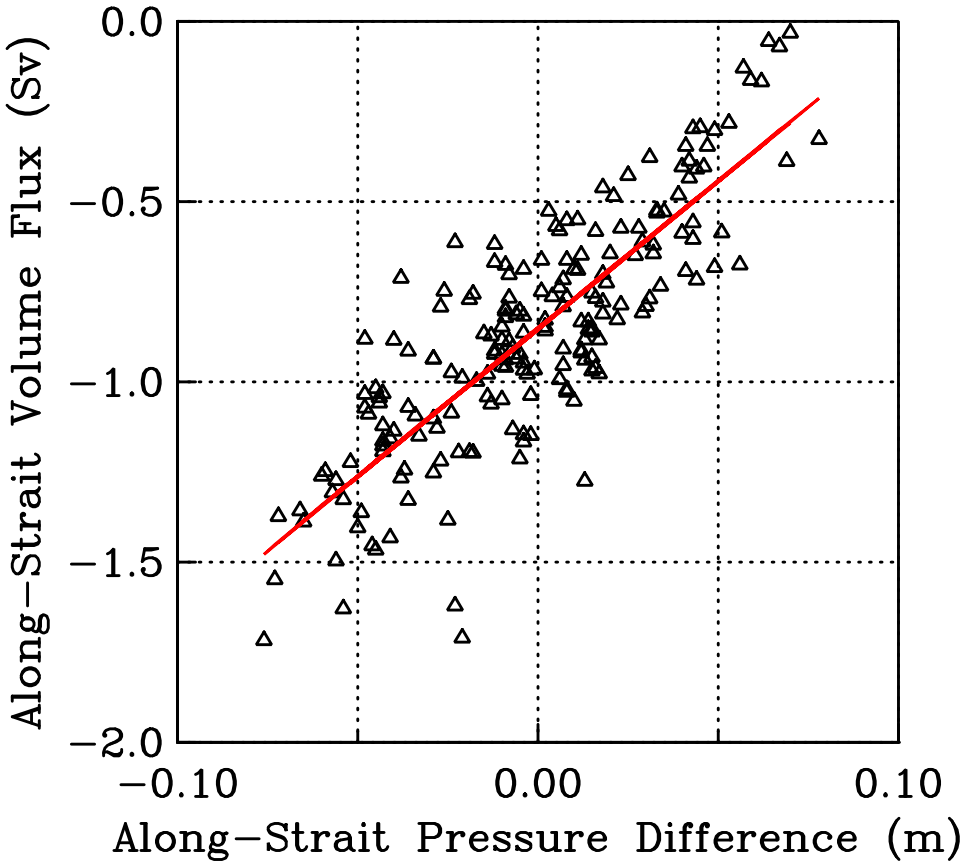

FIG. 11. Regression of along-channel pressure difference with volume flux.

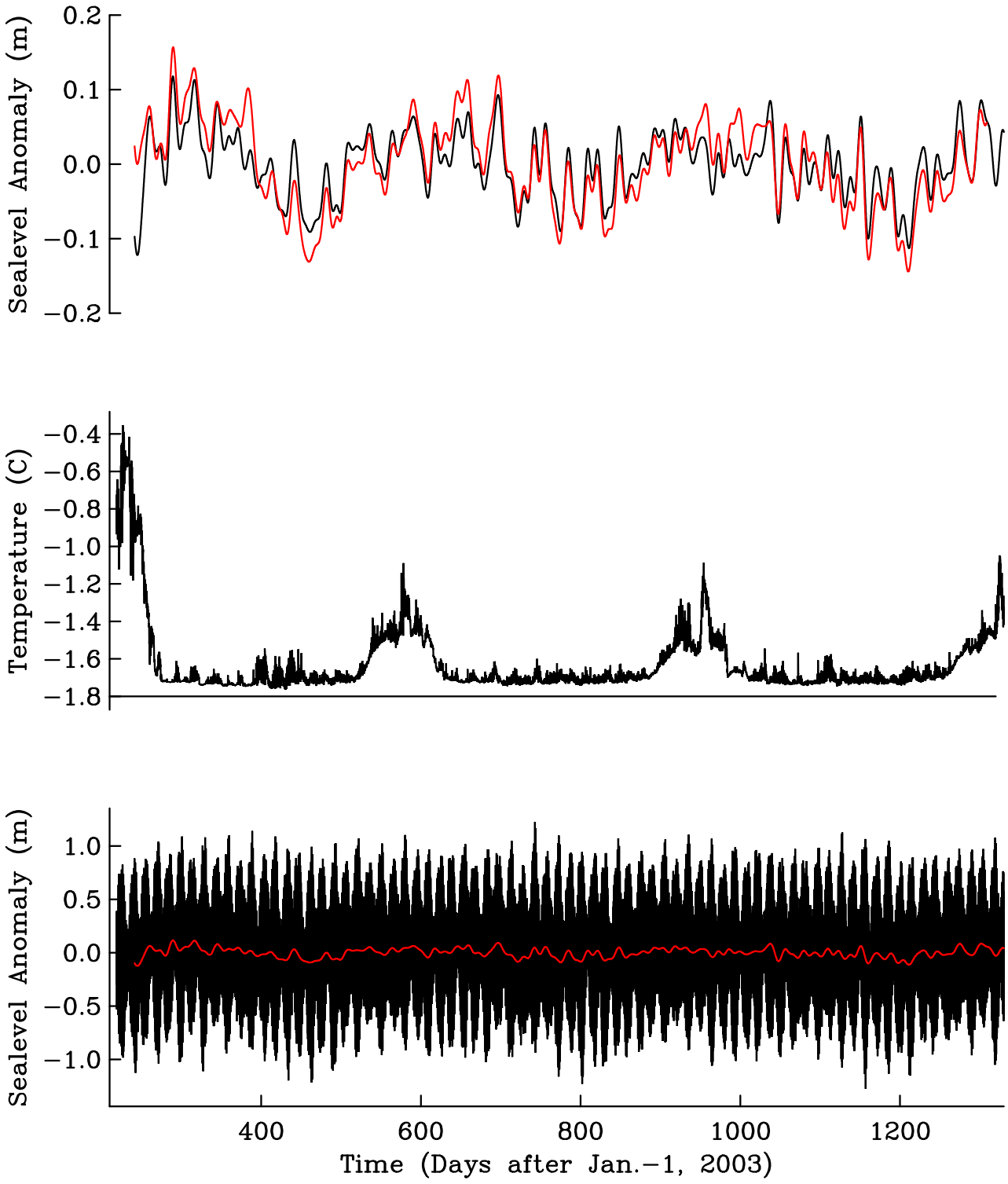

FIG. 12. Discovery Harbor sealevel (bottom), temperature (middle), and low-pass filtered sealevel anomaly (top) for Discovery Harbor and Alexandra Fjord (red) from 2003 through 2006.

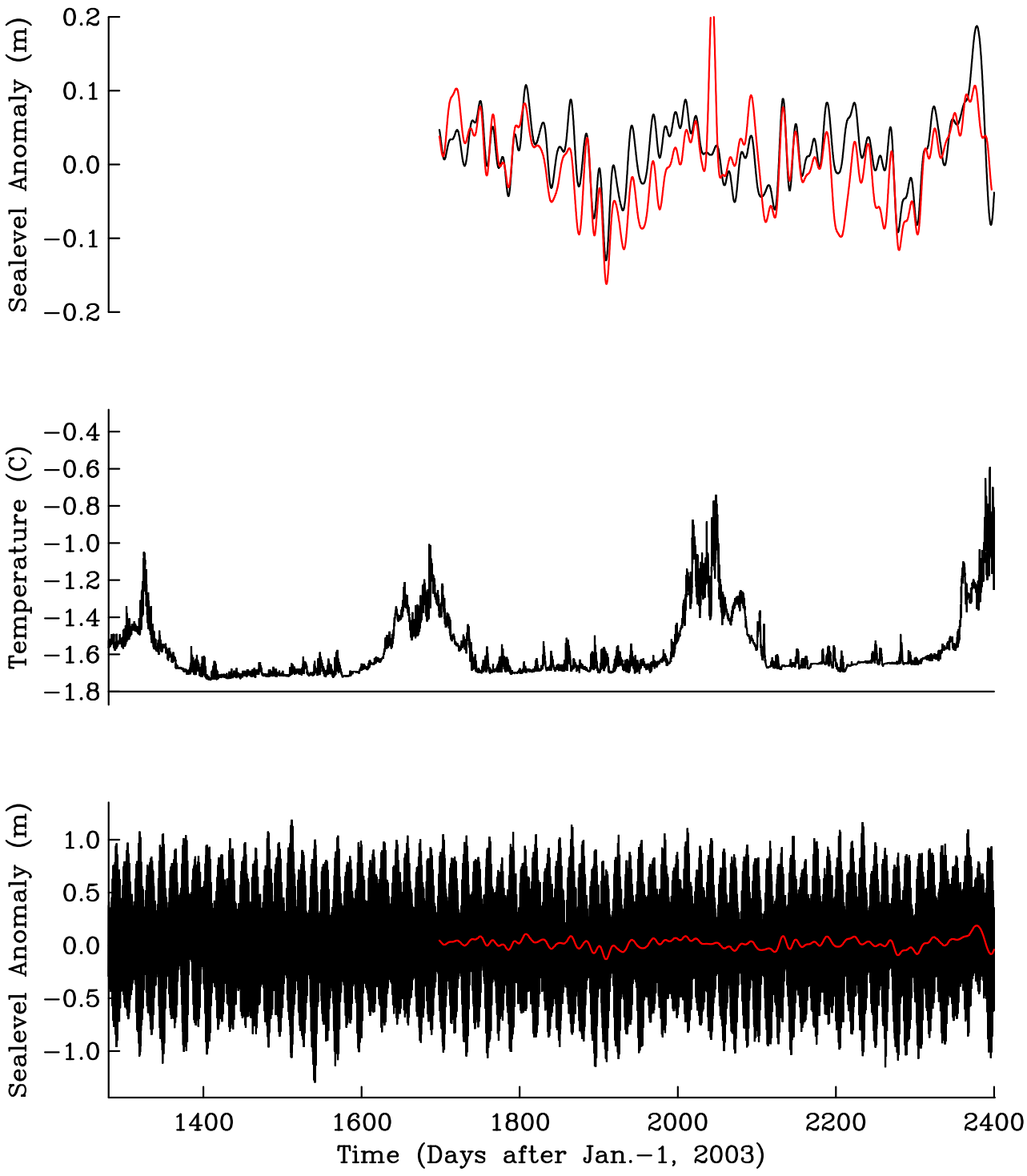

FIG. 13. Discovery Harbor sealevel (bottom), temperature (middle), and low-pass filtered sealevel anomaly (top) for Discovery Harbor and Alexandra Fjord (red) from 2007 through 2009.

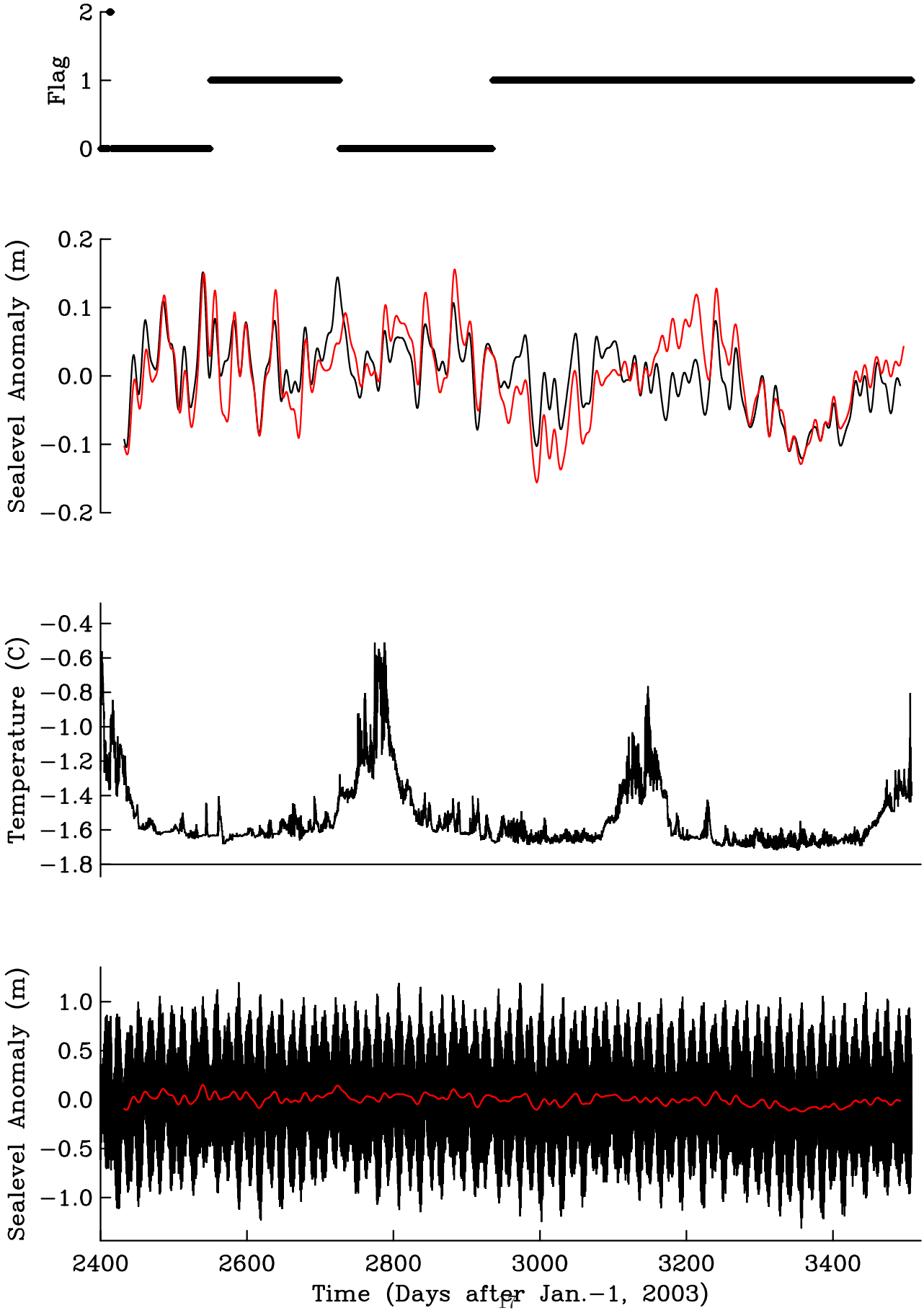

FIG. 14. Discovery Harbor sealevel (bottom), temperature (middle), and low-pass filtered sealevel anomaly (top) for Discovery Harbor and Alexandra Fiord (red) from 2009

TABLE 1. Amplitude A (in centimeter) and phase ϕ (in degrees) of tidal constituents from 2003-2012 observations In Nares Strait at Discover Harbor (A_N and ϕ_N at 81.7° N) and Alexandra Fjord (A_S and ϕ_S at 78.9°N). Uncertainties are less than ±0.01 cm for amplitude and less than ±3.3 degrees for phase at 95% level of confidence (Münchow et al. 1992).

Constituent	A_N	ϕ_N	A_S	ϕ_S	ϕ_N-ϕ_S	A_S/A_N
M_2	58.8	-75	130.7	-82	+7	2.2
S_2	27.1	-163	66.1	-176	+12	2.4
N_2	10.9	-157	25.6	-161	+4	2.3
K_2	9.2	44	17.7	41	+3	1.9
K_1	7.2	-114	32.1	-69	-45	4.5
O_1	2.6	-58	11.9	-13	-45	4.6
P_1	2.2	-127	9.4	-91	-36	4.3
S_a	2.1	103	4.5	98	+5	2.1
S_{Sa}	2.1	25	1.9	21	+5	0.9

TABLE 2. Mooring locations and records.

Name	Year	Latitude, N	Longitude, W	Depth, m	Record, days
Alert	2003-06	82.49	62.32	n/a	1120
Discovery Harbor	2003-12	81.71	64.80	28.70	3140
Alexandra Fjord	2003-06	78.91	75.81	34.40	1099
Alexandra Fjord	2007-09	78.90	75.83	25.61	730
Alexandra Fjord	2009-12	78.90	75.83	28.65	1096
Foulke Fjord	2003-06	78.30	72.57	35.62	1116